Adsorption of Nonionic Surfactant on Silica Nanoparticles: Structure and Resultant Interparticle Interactions

ARTICLE *in* THE JOURNAL OF PHYSICAL CHEMISTRY B · SEPTEMBER 2010

Impact Factor: 3.3 · DOI: 10.1021/jp1033799 · Source: PubMed

3 AUTHORS:

Kamendra Sharma
University of Bristol
21 PUBLICATIONS **131** CITATIONS
SEE PROFILE

Vinod K Aswal
Bhabha Atomic Research Centre
392 PUBLICATIONS **4,906** CITATIONS
SEE PROFILE

Guruswamy Kumaraswamy
CSIR - National Chemical Laboratory, Pune
46 PUBLICATIONS **1,230** CITATIONS
SEE PROFILE

Adsorption of Nonionic Surfactant on Silica Nanoparticles: Structure and Resultant Interparticle Interactions

Kamendra P. Sharma,[†] Vinod K. Aswal,[‡] and Guruswamy Kumaraswamy*,[†]

Complex Fluids and Polymer Engineering, National Chemical Laboratory (NCL), Pune 411008, India, and Solid State Physics Division, Bhabha Atomic Research Centre (BARC), Mumbai-400085 India

Received: April 15, 2010; Revised Manuscript Received: June 17, 2010

Addition of nonionic surfactant, $C_{12}E_9$, to an aqueous dispersion of charge stabilized silica nanoparticles renders particle aggregation reversible. In contrast, aggregation of the same silica particles in aqueous solutions is irreversible. We use a combination of small-angle X-ray scattering (SAXS) and contrast matching small-angle neutron scattering (SANS) to investigate interparticle interactions and microstructure in dispersions of silica particles in aqueous nonionic surfactant solutions. We show that the silica particles interact through a screened Coulombic interaction in aqueous dispersions; interestingly, this interparticle interaction is hard-sphere-like in surfactant solutions. In surfactant solutions, we show that the final surfactant−particle structure can be modeled as 14 micelles adsorbed (on average) on the surface of each silica particle. This gives rise to the short-range interparticle repulsion that makes particle aggregation reversible, and results in the hard sphere interparticle interaction potential. Finally, we show that adsorption of polyethylene imine on the surface of the silica particles prevents adsorption of surfactant micelles on the particle surface.

Introduction

We have recently reported[1] that electrostatically stabilized silica nanoparticles aggregate and form networks when a surfactant/water system containing these particles is cooled into the hexagonal (H_1) phase. Our work extended the previous understanding[2] of particle assembly in surfactant H_1 phases by systematically mapping the influence of particle size. Specifically, we have shown that particles over a wide size range (diameter, d, greater than 10 nm and up to about 500 nm; $d > a$, characteristic length scale of the H_1 phase; $a = 5.7$ nm, in our case) form such particulate networks in surfactant−water systems. This particle−particle aggregation into strands and into networks is driven by phase separation of the particles from the ordered H_1 phase. On cooling from the isotropic micellar phase, H_1 domains nucleate and grow, and expel the particles to the isotropic regions. Thus, as the isotropic regions shrink, the particles get concentrated, and eventually get jammed at the domain boundaries as the H_1 domains impinge. An intriguing aspect of this particle aggregation in the surfactant/water system is its thermoreversibility: On heating the particle−H_1 composite to above 44 °C, viz., above the H_1−isotropic transition temperature, the particulate network breaks up and redisperses into individual particles in the low viscosity micellar phase. Thus, the nanoparticles aggregate and disperse reversibly on cooling into the H_1 phase and on heating into the isotropic micellar phase, respectively. In contrast to this thermoreversibility in the surfactant micellar system, aggregation of charge stabilized silica particles from aqueous dispersions (for example, due to destabilization by increasing the ionic strength or changing the pH) was irreversible. Typically, for particle aggregation in aqueous dispersions, even vigorous sonication is unable to break up the aggregated particulate flocs. Thus, when particle aggregation in aqueous dispersions is irreversible, what is the origin of the thermoreversibility of aggregation of the same particles in surfactant solutions?

In this paper, we use SAXS and contrast matching SANS experiments to probe the change in nature of interparticle interactions for dispersions in water and in micellar solutions. We also investigate the microstructure of micelle−particle solutions to understand the origin of the interparticle interactions, and finally examine how coating the nanoparticles with polymers can alter this microstructure. Our results form the basis of our scheme to prepare self-standing nanoparticulate scaffolds that will be described elsewhere. We begin by briefly summarizing the relevant literature in the area of surfactant adsorption on colloids, before we describe our experimental system and our results.

Adsorption of surfactants and the role of surfactants in stabilizing colloidal dispersions has been studied extensively, as these phenomena are relevant to a range of industrial applications ranging from processing of minerals, cleaning and detergency, cosmetics and personal care applications, food products, pharmaceuticals, etc.[3] Specifically, nonionic surfactants find extensive use in the aforementioned applications, and there is a wealth of literature that describes their interactions with flat,[4−8] porous,[9−12] and colloidal surfaces.[5,13−15] Dispersion of colloids in surfactant solutions can dramatically influence colloidal stability, since surfactants interact strongly with colloidal surfaces. Therefore, a wide range of experimental techniques, including ellipsometry,[6] fluorescence decay spectroscopy,[9,16] atomic force microscopy,[17−20] dynamic light scattering,[5] small-angle neutron scattering,[13,15,21] neutron reflectivity,[4,5,7,22] etc., have been brought to bear on studies of surfactant adsorption on surfaces. Specifically, it is now understood that oligooxyethylene-based nonionic surfactants interact with silica surfaces by hydrogen bonding with the surface silanol groups. Nonionic surfactants with short hydrophilic oligooxyethylene headgroups, relative to the size of the hydrophobic tail, are believed to form bilayers on adsorption on surfaces.[4] However, several groups have also reported that,

* Corresponding author. Phone: +91-20-2590-2182. Fax: +91-20-2590-2618. E-mail: g.kumaraswamy@ncl.res.in.
[†] NCL.
[‡] BARC.

10.1021/jp1033799
Published on Web 08/05/2010

rather than forming bilayers, the nonionic surfactants adsorb on surfaces in the form of micellar structures.[9,15,16,23−25] The group of Levitz has suggested that the formation of the adsorbed micellar structures on surfaces proceeds via the initial adsorption of surfactant molecules on the surfaces, and their subsequent reorganization into micellar structures. Alexeev et al.[25] suggest that the stability of silica nanoparticles in nonionic surfactant solutions depends on the extent of surface coverage by surfactant micelles—they claim that nanoparticle dispersions are stable so long as there is at least one layer of surfactant micelles that separates the nanoparticles.

Thus, it is clear that surfactant−nanoparticle interactions, and the structures that form as a consequence of these interactions, critically determine the phase behavior of nanoparticle dispersions in surfactant solutions. In this work, we focus on interparticle interactions in surfactant solutions, and relate these to the surfactant/particle microstructure.

Experimental Details

Nonionic surfactant, nonaethylene glycol dodecyl ether ($C_{12}E_9$), was obtained from Sigma Aldrich and was used as received (HPLC previously reported[26]). Distilled deionized water (resistivity = 18.2 MΩ·cm) from a Millipore Milli-Q unit was used to prepare all samples. Polyethylene-imine (PEI) was obtained from Aldrich as a 50% (by weight) solution with a weight average molecular weight of 2000 g·mol^{-1}. All of the chemicals were used as received.

An electrostatically stabilized 30% (by weight) colloidal suspension of silica particles, Ludox-LS30 was obtained from Sigma Aldrich. We have thoroughly characterized the Ludox-LS30 particles using DLS, SAXS, and TEM and have reported these data previously.[1] TEM indicates that these particles are approximately spherical, with an average particle diameter of around 12 nm, in accord with the manufacturer's specification. However, the particle size obtained by fitting the DLS data and by fitting the SAXS form factor is larger than the TEM, possibly due to shrinkage of the particles during sample preparation for TEM imaging. Our SAXS data for the form factor of the particles can be fitted assuming that the particle sizes follow a log-normal distribution with a diameter of ∼15 nm and a standard deviation of 0.14 (Figure 1, inset). Therefore, here, we refer to these particles as S15 (viz., silica particles with an average diameter of 15 nm).

The surface of S15 was coated with PEI according to a procedure reported in the literature.[27] We maintain pH 5 when S15 is coated with PEI to enable protonation of the amine groups on the PEI, since PEI−S15 interactions are believed to be driven by electrostatics. The ratio of PEI to S15 was chosen so as to have a surface coverage of 0.1 mg/m^2 (calculated assuming the manufacturer specified surface area of 220 m^2/g for S15). PEI coated S15 particles are referred to as PEI−S15 and are characterized using SAXS (to determine the size) and using zeta potential measurements (on a Brookhaven Zetasizer, to determine the surface charge).

SAXS measurements were performed on a Bruker Nanostar equipped with a rotating anode generator (18 kW) operated at a voltage of 45 kV and current of 100 mA. The X-rays are collimated through a three-pinhole system, and data is acquired using a 2D gas filled Hi-Star detector over a q-range of 0.011−0.2 Å^{-1}. The detector was calibrated using a silver behenate sample. Samples were sealed in quartz capillaries having an outer diameter of 2 mm and wall thickness of ≈10 μm. Data was corrected for background scattering (including solvent scattering and air scattering). The 2D data were reduced to 1D by circularly averaging, using the software provided with the instrument.

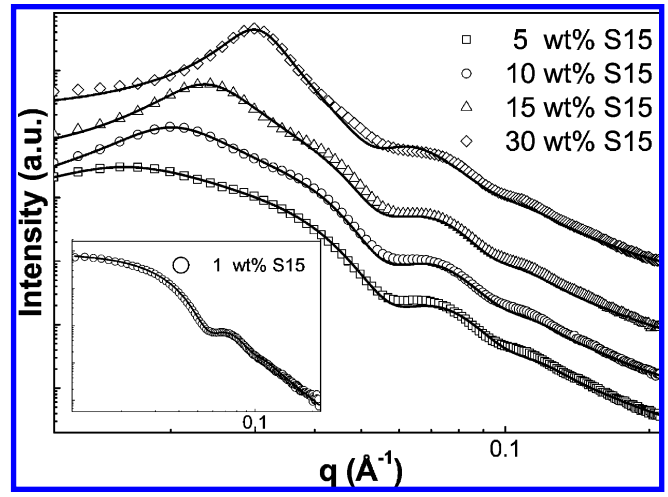

Figure 1. SAXS data at different concentrations of S15 (5, 10, 15, and 30%, by weight) in water at 50 °C. The data was fitted (solid lines) assuming screened Coulombic interactions between the charged particles using a Hayter−Penfold model, as described in the text. For ease of viewing, the data plots have been vertically offset by multiplying with 1, 4, 20, and 200 for 5, 10, 15, and 30%, respectively. The inset shows the scattering from a dilute solution (1% by weight) of S15 in a 25 mM solution of sodium chloride. The fit through the data is shown as a solid line.

SANS measurements were done at the beamline in the Dhruva Nuclear Reactor at Bhabha Atomic Research Centre, Mumbai. The wavelength of the neutron beam was 5.2 Å, and the q range of scattering was 0.017 to 0.34 Å^{-1}. Samples were contrast matched by tuning the ratio of H_2O and D_2O in the solvent so as to match the scattering length densities of the solvent with either the silica particle or the surfactant, $C_{12}E_9$. All samples were equilibrated for at least 12 h before measurements. Measurements were performed with 2 mm thick quartz cuvettes. All of the data sets were normalized with the beam monitor and the sample volume and were background corrected to obtain the scattering cross section. The scattering data was reduced to an absolute cross section (in cm^{-1}) by reference to scattering from a standard sample. Fits to the SANS are convoluted with the resolution function obtained previously[28] to account for the wavelength spread ($\Delta\lambda/\lambda$) and the neutron beam angular resolution.

Data analysis was performed using codes written in our laboratory, and the results were compared, in some cases, with analysis using SASfit.[29] As the results were comparable, here, we report only the analysis based on our routines.

Results and Discussion

Our results are divided into three parts. We begin with SAXS and SANS investigations of particle−particle interactions in water and in isotropic micellar solutions. We then investigate structure in the micelle−particle system using SANS. Finally, we describe the structure observed in micellar solutions containing PEI coated silica nanoparticles.

S15 particles are electrostatically stabilized. At dilute concentrations (1% by weight, viz., approximately 0.5% by volume), in solutions containing salt (25 mM sodium chloride, added to screen the range of electrostatic interparticle interactions), we obtain the SAXS form factor, $F^2(q)$, for S15 (Figure 1, inset). We have verified that scattering profiles from solutions at lower particle concentrations can be superposed with the form

TABLE 1: Parameters from Fitting a Structure Factor for Screened Coulombic Interactions (Based on the Hayter−Penfold Model)[a]

			parameters from fitting structure factor, $S(q)$				
sample (S15, % by weight)	measured ionic strength (μS/cm)	ϕ_e	ϕ_f	r_{HPY} (Å)	κ^{-1} (Å)	potential ψ_0 (mV)	particle charge (in e.u.)
5	201	0.023	0.024	78.5	154.8	46.7	31.1
10	388	0.049	0.055	80.6	96.0	46.0	37.4
15	601	0.074	0.10	82.8	66.8	45.6	46.3
30	1357	0.164	0.22	84.5	41.5	41.4	58.1

[a] We use a form factor based on fitting data to a 1% (by weight) dispersion of S15 in 25 mM aqueous solution, that gives an average particle radius of 74.5 Å, and a log-normal distribution of radii with $\sigma = 0.14$ and ionic conductance of 62.8 μS/cm.

factor in Figure 1, inset, after normalization with the particle volume fraction. We can fit the form factor for S15 assuming that the particles are spherical (this is a reasonable assumption based on TEM results[1]), and follow a log-normal distribution of sizes with a mean radius (R_{S15}) of 74.5 Å and a standard deviation of 14%. Thus, the S15 particles are not monodisperse (but have a *unimodal* size distribution) and the form factor obtained experimentally, $F^2(q)$, is an *average* over the S15 particle size distribution.

As the particle volume fraction is increased, to 5, 10, 15, and 30% (by weight), interparticle interference increases, resulting in a structure factor, $S(q)$, that becomes increasingly prominent with an increase in particle concentration (Figure 1; note that no salt is added to prepare these dispersions). For an isotropic dispersion of monodisperse particles, $S(q)$ is given by the Fourier transform of the particle radial distribution function. In this case, $S(q)$ can be calculated from the Ornstein−Zernike equation, with an appropriate closure relation, and by assuming a suitable form for the interparticle interaction. An excellent review of this analysis and the commonly made assumptions, especially in the context of polydisperse colloidal and micellar systems, is given in the chapter by Kaler.[30] Thus, we write the scattered intensity, I, as

$$I = \Delta\rho^2 \phi V_s \hat{S}(q) F^2(q) \quad (1)$$

where $\Delta\rho$ is the contrast between the scatterer and the matrix (electron density difference, in the case of SAXS and scattering length density difference in the case of SANS), ϕ is the volume fraction of the scatterer, V_s is the scattering volume, and $\hat{S}(q)$ is the "apparent" structure factor that averages over the interactions between the polydisperse S15 particles, viz., $\hat{S}(q)F^2(q) = \sum_i \sum_j F_i F_j S_{ij}$, where the indices i and j are summed over all S15 particles and S_{ij} is the structure factor. Thus, we model the experimental scattered intensity with the average form factor for polydisperse spherical particles and with an apparent structure factor that assumes monodisperse spherical scatterers. Assuming a hard sphere interparticle interaction potential yields an analytical expression for the apparent structure factor.[31] We observe a reasonable fit to our data, with the experimentally obtained form factor and with a structure factor based on an effective hard sphere model for the interparticle potential (Supporting Information, Figure S1). The particle radius predicted by the effective hard sphere model is larger than the experimental value, since it accounts for the electrostatic repulsion between the charged particles, and accordingly the predicted volume fraction is also larger than the experimental value. However, the values of the best fit hard sphere radius and volume fraction are not physically realistic (Supporting Information, Table S1), since, for example, the discrepancy between the fitted volume fractions and hard sphere radii and the experimental values increases with the concentration of nanoparticles in the dispersion, while one would expect the opposite trend for the effective hard sphere model.[32a,b] Therefore, we are unable to model the scattering from our system using an effective hard sphere potential to represent interparticle interactions.

TABLE 2: Parameters from Fitting a Structure Factor Based on Hard Sphere Interparticle Interactions[a]

		parameters from fitting structure factor, $S(q)$	
sample (S15, % by weight)	ϕ_e	ϕ_f	R_{HS} (Å)
5	0.023	0.025	81.4
10	0.049	0.048	78.7
15	0.074	0.087	77.5

[a] We use a form factor based on fitting data to a 1% (by weight) dispersion of S15 in 25 mM aqueous solution, that gives an average particle radius of 74.5 Å, and a log-normal distribution of radii with $\sigma = 0.14$.

For electrostatically stabilized particles dispersed in a buffer, one might imagine that particles interact via a soft exponentially decaying potential of the form $U \sim r^{-1}e^{-\kappa r}$, where κ is the inverse Debye screening length set by the ionic strength of the solution.[33] Therefore, we fit our data using an apparent structure factor from the Hayter−Penfold model[34] that assumes that the silica nanoparticles interact via a screened Coulombic interaction potential. The form of the potential is similar to the Yukawa model and is given by

$$U(r) = 2\pi\varepsilon_0\varepsilon r_{HPY}^2 \psi_0^2 \exp[-\kappa(r - 2r_{HPY})]/r \quad (2)$$

where ε_0 is the permittivity of free space, ε is the dielectric constant of water, r_{HPY} is the particle radius, and ψ_0 is the electrostatic potential of the silica nanoparticles. This model fits the data reasonably well (Figure 1) at low q, and the fit parameters are summarized in Table 1. At high q, near the first oscillation in the structure factor, the fit to the data is not perfect. We attribute this to two possible reasons: (a) limitations in modeling the data using an *effective* structure factor, and accounting for the effect of the polydispersity only in the form factor, especially for higher particle volume fractions and (b) problems associated with subtracting the background intensity from the acquired data, prior to normalization with particle concentration. We note that the samples are prepared by diluting the 30% (by weight) S15 dispersions with distilled, deionized water. We observe a decrease in conductivity on diluting the S15 dispersion (reported in Table 2). The trends in the fitted parameters with concentration broadly accord with previous findings.[35]

We now consider scattering from silica particles in a matrix comprising equal weight fractions of nonionic surfactant, $C_{12}E_9$,

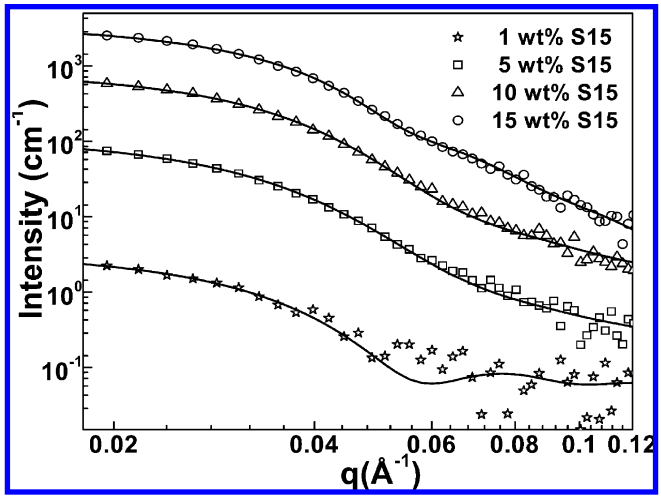

Figure 2. SANS data from dispersions of S15 particles at concentrations of 1, 5, 10, and 15%, by weight) in contrast matched 1:1 $C_{12}E_9$: (97.5% H_2O−2.5% D_2O) micellar solutions, at 50 °C. The data sets for 1, 5, 10, and 15 wt % have been vertically offset by multiplying with 0.5, 3, 12, and 40, respectively, for ease of viewing. Since the particles are supplied in a 30% by weight solution, the highest concentration possible in 1:1 surfactant solution is about 15% by weight.

and water. We have previously shown[1] that S15 particles form transparent dispersions in 1:1 $C_{12}E_9$/water at high temperature (50 °C), indicating that the particles are well dispersed. For example, SAXS from a 1% dispersion of S15 in 1:1 $C_{12}E_9$/water at 50 °C shows the form factor for the S15 and a micellar correlation peak.[1] On cooling, the surfactant goes from a low viscosity solution to a gel, due to the formation of a hexagonal (H_1) mesophase (the phase behavior of $C_{12}E_9$/water[36] and also for other surfactants of the C_nE_m type has been described previously[6,37]). When the H_1 phase forms, the particles are expelled from the H_1 domains and aggregate at the domain boundaries, giving rise to a pronounced structure factor in SAXS.[1] On heating back into the isotropic micellar phase, the particles redisperse and we recover the form factor. This is very unlike the aggregation of S15 particles in water, where destabilization, for example, by increasing the ionic strength or by changing the pH, leads to irreversible particle aggregation. Therefore, clearly, there is a change in particle−particle interactions in the surfactant micellar phase, resulting from the structure of the $C_{12}E_9$/water/particle system. Therefore, we now investigate the surfactant/water/particle system at high temperature (50 °C), in the low viscosity, isotropic micellar phase.

In the micellar phase, $C_{12}E_9$ aggregates to form a hydrophobic core of C_{12} segments and a solvated shell of the E_9 segments. Therefore, for our SANS studies, we adjust the water/D_2O composition in our surfactant formulation so as to contrast match the aliphatic C_{12} micellar core (97.5% H_2O, 2.5% D_2O; scattering length density = -3.86×10^{-7} Å^{-2}). We confirm that the micelles are, indeed, contrast matched at this water/D_2O concentration−SANS from these micellar solutions yields a very low scattered intensity, arising mainly from the incoherent background (Supporting Information, Figure S2). SANS data from dispersions of S15 particles (at concentrations of 1, 5, 10, and 15%, by weight) in contrast matched 1:1 $C_{12}E_9$:(97.5% H_2O−2.5% D_2O) micellar solutions is shown in Figure 2. We first fit the SANS data (Figure 2) for 1% S15 dispersions using a spherical form factor averaged over a polydisperse size distribution and note that the average particle size and polydispersity obtained from our fit (Table 2) accord very well with that obtained from the SAXS for S15 in water (compare with

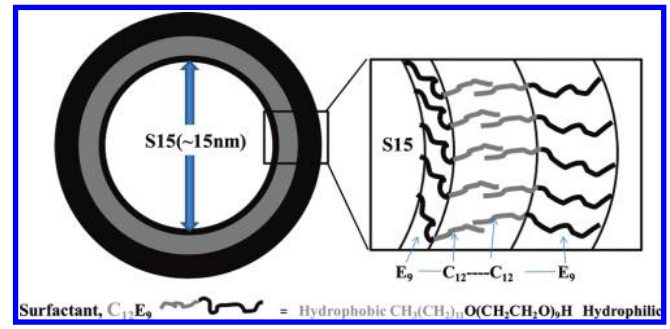

Figure 3. Schematic of surfactant adsorbed as a bilayer "shell" on a nanoparticle surface. The ethylene oxide segments are shown in dark, while the hydrophobic segments are indicated in light lines.

Table 1). We fit the SANS data at higher S15 concentations (5% and higher) with the obtained form factor and by assuming an apparent structure factor for monodisperse particles. Interestingly, the SANS data is fitted very well assuming hard sphere interparticle interactions. The volume fraction, ϕ_f, obtained by fitting the apparent structure factor accords reasonably well with the experimental values, ϕ_e. At the highest particle concentration, the fitted value ($\phi_f = 0.087$) is higher than the experimental value ($\phi_e = 0.074$) by about 17.6%. We believe that this difference may be attributed to the error from averaging the interparticle interactions into an apparent structure factor. The hard sphere radius obtained by fitting the apparent structure factor (viz., the length scale over which particles interact) is similar at all particle concentrations, and is within 10% of the particle radius from the form factor, as expected for particles interacting through a hard sphere potential (Table 2). At the high surfactant concentrations investigated here (50% by weight), "crowding" effects[38] due to the large number density of surfactant micelles that surround the silica particles influence interparticle interactions. Further, we expect that the effective dielectric properties of the surfactant/water matrix are considerably different from that of pure water, and influence the interparticle electrostatic interactions. Finally, we anticipate surfactant−particle interactions in our system based on the surfactant chemistry and the particle surface chemistry. Interestingly, we observe that, taken together, these effects result in an effective hard sphere interaction between the silica particles. We note in passing that, at intermediate surfactant concentrations of a few percent, depletion interactions due to the micelles result in interparticle attraction and lead to gelation at high particle concentrations. We are currently investigating this phenomenon in detail and will report our results in future publications.

To understand the structural underpinning of the change in interparticle interaction between the silica particles on addition of surfactant, we investigate surfactant organization in the dispersion. We anticipate that surface silanol groups on the S15 particles would interact with the ethylene oxide segments of $C_{12}E_9$. Intuitively, one might imagine the formation of a surfactant bilayer on the S15 surface, with a hydrophobic shell comprised of C_{12} segments sandwiched between layers of ethylene oxide segments, the inner layer adsorbed on the S15 surface, and the solvated outer layer in contact with water (see the schematic in Figure 3). If we contrast match the silica particle (scattering length density = 3.59×10^{-6} Å^{-2}) by working in a 40/60 mixture of water and D_2O, we obtain the scattered intensity as[31]

$$I = \Delta\rho^2 \nu_m \hat{S}_{mm}(q) F_m^2(q) + \Delta\rho^2 \nu_s \hat{S}_{ss}(q) F_s^2(q) + 2\Delta\rho^2 (\nu_s \nu_m)^{0.5} \hat{S}_{sm}(q) F_s(q) F_m(q) \quad (3)$$

where the subscripts m and s refer to the micelle and the surfactant shell, respectively, ν_x is the number density of the scattering species, x, and $\hat{S}_{xy}$ are the apparent partial structure factors (averaged over the polydisperse size distribution) for interference between scattering species, x and y. The scattered intensity has contributions from surfactant micelles and the intermicellar apparent structure factor, $\hat{S}_{mm}$; from the surfactant "shells" around S15 particles and from shell−shell interference, $\hat{S}_{ss}$; and from interference between micelles and shells, $\hat{S}_{sm}$. As the silica is contrast matched with water/D_2O, and since the ethylene oxide segments are solvated, the neutron scattering in our experiments is primarily from the structures formed by the hydrophobic C_{12} segments (viz., the micellar cores and the hydrophobic part of the shells). Typically, determining partial structure factors in multicomponent systems requires contrast variation experiments on the same sample to generate multiple data sets that are fitted simultaneously.[31] However, in our experiments, the different scattering entities (viz., the micelles and the surfactant shells) have the same scattering length density difference, $\Delta\rho$, with respect to the solvent (see eq 3). Thus, it is not possible to extract partial structure factors for our system, even with contrast variation experiments. Therefore, to extract meaningful information about our experimental system, we design our samples such that $\hat{S}_{mm}$ is close to 1 and $\hat{S}_{sm}$ is close to 0.

Concentrated surfactant solutions, for example, the 1:1 $C_{12}E_9$: (water/D_2O) system that we have described earlier, have a large number density of micelles, and therefore, in such systems, S_{mm} is not expected to be close to 1. SANS from 1, 5, and 10% (by weight) $C_{12}E_9$ solutions (not containing S15) show that the scattering can be described by the form factor of the micellar core for 1 and 5% solution (viz., $\hat{S}_{mm}(q) = 1$; Figure S3 in the Supporting Information, size of hydrophobic core of micelle = 19.1 Å). For the 10% solution, the scattering can be modeled only if we consider a micelle−micelle apparent structure factor based on a hard sphere interaction between the micelles (viz., we cannot assume that $\hat{S}_{mm}(q) = 1$; Figure S3 in the Supporting Information). Therefore, we only consider scattering for systems where the surfactant concentration does not exceed 5%. Further, we assume that, at these surfactant concentrations, where $\hat{S}_{mm}(q) = 1$, we can also neglect the micelle−shell term, viz., $(\nu_s \nu_m)^{0.5} F_s(q) F_m(q) \hat{S}_{sm}(q) = 0$. We return to this point and justify our assumption later.

We initially examine scattering from a 1% (by weight) dispersion of S15 in a solution containing 1% (by weight) surfactant (that we term a "1%1%" sample) in water/D_2O (with scattering length density matched to silica). At these particle and surfactant concentrations, we assume that there is no contribution from the apparent partial structure factors (viz., $\hat{S}_{ss}(q) = \hat{S}_{mm}(q) = 1$ and $\hat{S}_{sm}(q) = 0$), and the scattering comes only from the micellar and shell form factors (averaged over their size distributions, respectively). Thus, the 1%1% sample is comprised of a *dilute* solution of micelles and shells and there is no interference between the scattering from these. The SANS data from the 1%1% sample is fitted well (Figure 4a), and the fit parameters are summarized in Table 3. When fitting the experimental data, we fix the inner size of the shell as R_o = 74.5 Å, based on the average particle size from the form factor, R_{S15}. Our fit yields an average shell thickness R_s of 36.1 Å and an average micellar radius of R_m = 18.4 Å.

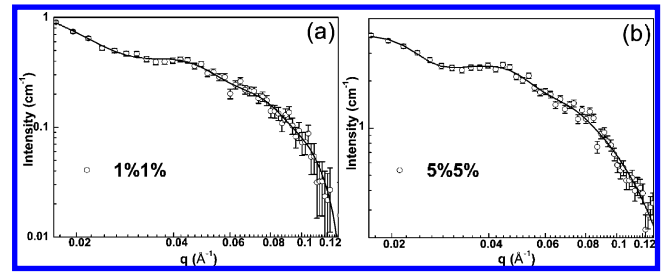

Figure 4. SANS from (a) 1%1% sample and (b) 5%5% sample (see text) at room temperature. Fits through the data using the core−shell model for adsorbed surfactant are given as solid lines.

TABLE 3: Fit Parameters for the Core−Shell Model of Surfactant Adsorption on S15 (Data Presented in Figure 4)

sample	R_m (Å)/σ	ν_m (cm^{-3})	R_s (Å)	ν_s (cm^{-3})	R_{HS} (shell−shell interaction) (Å)	ϕ_f
1%1%	18.4/0.24	3.15×10^{17}	36.1	4.55×10^{13}		
5%5%	18.7/0.30	2.1×10^{18}	36.8	2.9×10^{14}	121.6	0.23

For scattering from a 5% dispersion of S15 in a 5% surfactant solution (a "5%5%" sample), we are unable to fit the SANS data with just the micelle and shell form factors. As the micelle−micelle apparent structure factor for a 5% surfactant solution in water is equal to 1 (Supporting Information, Figure S3), we assume that the apparent partial structure factor, $\hat{S}_{mm}(q)$, is also equal to 1. We note that the size of the surfactant bilayer "shell" is large compared to a micelle (see Table 3; the shell forms around the S15 particle with diameter ≈ 15 nm). Therefore, we attempt to fit the 5%5% data assuming interference between the scattering from shells, and by modeling an apparent partial structure factor, $\hat{S}_{ss}(q)$, assuming that the potential of mean force between the shells is a hard sphere potential. Our data is fitted well, with an average R_s = 36.8 Å and an average R_m = 18.7 Å, in good accord with the fit to the 1%1% data (Figure 4b). The fitted structure factor gives a hard sphere radius (R_{HS}) of 121.6 Å for the shells, a value that is slightly larger than 111.3 Å (=$R_o + R_s$)—this is reasonable, since the shells interact through the hydrated ethylene oxide segments.

Since our SANS data is normalized to absolute intensity, we can calculate the surfactant concentration that is required to form the shells and micelles in our model structure. We assume a density, ρ, of 750 kg·m^{-3} (=the density of dodecane) for the density of the condensed hydrocarbon phase for the aliphatic chains in the shell and in the micellar core and calculate the surfactant concentration as $[\nu_m(4/3)\pi R_m^3 \rho + \nu_s 4\pi R_o^2 R_s \rho] M_s / M_{HC}$, where M_s is the molecular mass of $C_{12}E_9$ (582 g·mol^{-1}) and M_{HC} (169 g·mol^{-1}) is the molecular mass of the aliphatic C_{12} chain. For the 1%1% system, this yields a calculated surfactant concentration of 2.17%, while, for the 5%5% system, this yields a calculated surfactant concentration of 15%, well in excess of the experimental quantities (details of calculation in the Supporting Information). Therefore, it appears that our model of the surfactant adsorbing onto the silica particles to form a bilayer shell does not describe our system accurately. This conclusion accords with recent work by Oberdisse et al.[15,23,24] who have examined a variety of surfactant−silica nanoparticle systems and have shown that these systems are best described as micelles that are adsorbed onto the nanoparticle surface (rather than an adsorbed bilayer surfactant shell). In the work of Oberdisse et al.,[24] the scattering data at high q (>0.08 Å^{-1}) are not described by a model of surfactants adsorbing to form a shell. We note that our model of scattering from

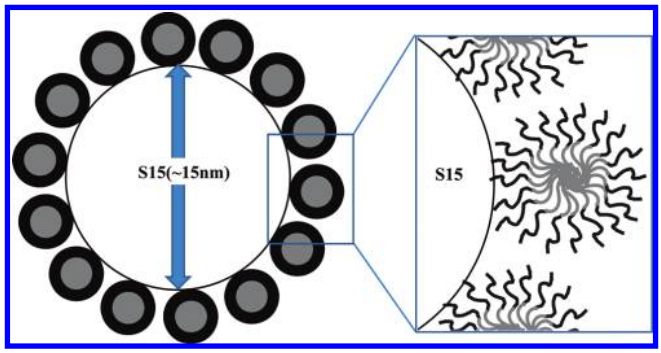

Figure 5. Schematic of surfactant adsorbed as a micelle on a nanoparticle surface. The ethylene oxide segments are shown in dark, while the hydrophobic segments are indicated in light lines.

individual micelles and adsorbed surfactant shells fits our experimental SANS data over the entire range of q. However, the large discrepancy between the surfactant concentration calculated from our model fits and the experimental values clearly indicate that the adsorbed surfactant shell model provides an inaccurate description. We also contrast the surface coverage of the surfactant calculated from our model fit to data from adsorption isotherms. Data for adsorption of $C_{12}E_9$ on silica is not available in the literature; however, adsorption isotherm data for $C_{12}E_8$ and for a family of $C_{12}E_m$ have been previously reported.[5,6,24] On the basis of this data, we estimate that the saturation surface coverage of $C_{12}E_9$ adsorbed on our particle surface is between 1 and 2 μmol·m^{-2} (viz., ≈0.6−1.2 mg·m^{-2}) and that the particle surface is saturated at a bulk surfactant concentration of about 0.1 mmol·L^{-1} (viz., ≈0.06%). Thus, at the surfactant bulk concentrations that we use in our work, we expect saturation surface coverage. Our fit, using the bilayer model, indicates a surfactant surface coverage of 14.6 mg·m^{-2}, vastly higher than the value expected from the adsorption isotherms (see calculations in the Supporting Information). Therefore, we now model our data using an alternate model, the adsorbed micelles picture suggested by Oberdisse et al.[15]

In the adsorbed micelle model, we assume that n_a micelles are adsorbed on average on each silica particle. It is to be noted that we do not imply that the surfactants assemble into micelles in solution, and subsequently adsorb on the particle surface as discussed in the pioneering work by Levitz.[9,39] We refer only to the final structure of the surfactant−particle system. Thus, the scattered intensity arises from free micelles in solution and from adsorbed micelles, and we also account for the interference between these (see the schematic in Figure 5). The scattered intensity can, thus, be written as

$$I = \Delta\rho^2 \nu_m \hat{S}_{mm}(q) F_m^2(q) + \Delta\rho^2 \nu_p \hat{S}_{pp}(q) n_a \hat{S}_{aa}(q) F_a^2(q) + 2\Delta\rho^2 (\nu_p n_p \nu_m)^{0.5} \hat{S}_{am}(q) F_a(q) F_m(q) \quad (4)$$

where ν_p is the number of silica particles, $F_a^2(q)$ is the form factor of the adsorbed micelles, $\hat{S}_{aa}(q)$ accounts for the interference from micelles adsorbed on a single particle, and $\hat{S}_{pp}(q)$ accounts for interference between micelles adsorbed on different particles. $\hat{S}_{am}(q)$ is an apparent partial structure factor that accounts for interference between free micelles and adsorbed micelles. The other symbols have the same meaning as defined earlier. To fit our data, we simplify our model by assuming that the adsorbed micelles have the same structure as the free micelles, viz., $F_a^2(q) = F_m^2(q)$. Further, recalling that, in solutions of up to 5% surfactant in water, we can model the scattering with only the micellar form factor (viz., without recourse to a structure factor), it is reasonable that $\hat{S}_{mm}(q) = 1$ and $\hat{S}_{am}(q) = 0$ at the relatively dilute concentrations of surfactant and silica particles in our experiments. We model $\hat{S}_{aa}(q)$ as suggested by Oberdisse et al. Briefly, we randomly place n_a micelles on the surface of a silica particle and calculate the structure factor as in eq 5 (viz., by assuming that the vector, $\mathbf{r}_i - \mathbf{r}_j$, is isotropically distributed), and simulate $\hat{S}_{aa}(q)$ by averaging over 10000 realizations.

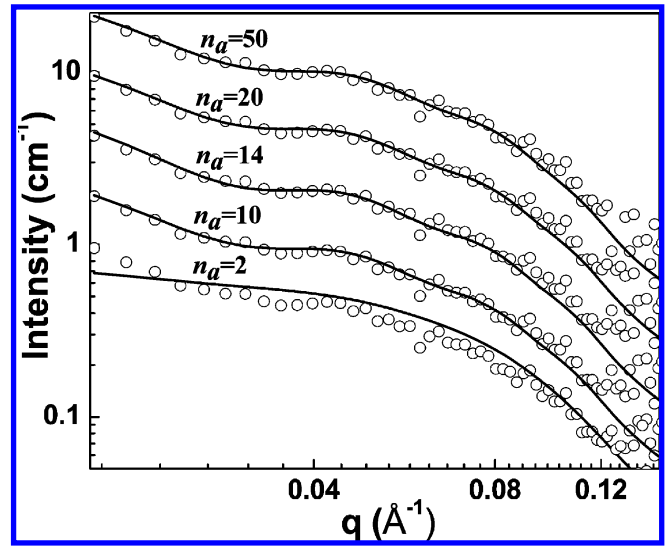

Figure 6. SANS from 1%1% sample at room temperature and fits corresponding to the adsorbed micelle model for n_a = 2, 10, 14, 20, and 50 micelles. The data (and fits) for different n_a are vertically shifted for clarity.

$$\hat{S}_{aa}(q) = 1 + \frac{1}{n_a} \sum_{i=1}^{n_a} \sum_{j>i}^{n_a} \frac{\sin(q(r_i - r_j))}{q(r_i - r_j)} \quad (5)$$

Thus, the scattering from our dispersion simplifies to

$$I = \Delta\rho^2 F_m^2(q)[\nu_m + \nu_p \hat{S}_{pp}(q) n_a \hat{S}_{aa}(q)] \quad (6)$$

For a particle radius of ≈75 Å and a micellar radius of ≈20 Å, we can accommodate a maximum of ∼O($4R_o^2/R_m^2$ = 56) micelles. Therefore, we have simulated $\hat{S}_{aa}(q)$ for different numbers of adsorbed micelles, n_a (=2, 10, 14, 20, 50), and have fitted the scattering data for each guess value of n_a (simulated $\hat{S}_{aa}(q)$ shown in the Supporting Information as Figure S5).

For the 1%1% system, we assume that $\hat{S}_{pp}(q) = 1$ as the nanoparticle concentration is dilute and present fits to the data for n_a = 2, 10, 14, 20, and 50 (Figure 6). We constrain the average particle size, R_o, to the value obtained by fitting the form factor for the particles (R_{S15}, see Tables 1 and 2) and fit the data to eq 6 for various values of n_a. We see that the data is not fitted well for n_a = 2; however, for the other values of n_a, the quality of the fit is good and the dip around q = 0.04 Å^{-1} is reproduced (Figure 6). Our data is fitted well with an average micellar radius of 19−20 Å. We calculate the surfactant concentration based on our fits for different values of n_a and observe that our experimental values are most closely reproduced for n_a = 14 (Table 4; for details of calculation, see the Supporting Information). Further, we observe that the number density of particles, ν_p, from our fit closely matches the average number of silica particles for a 1% dispersion of particles (Table

TABLE 4: Fit Parameters for the Adsorbed Micelle Model (Figure 5) for Different Values of n_a[a]

n_a (1%/1% sample)	ν_m (cm^{-3})	ν_p (cm^{-3})	calculated surfactant concentration (mg/mL)	under (+)/over (−) estimation of surfactant concentration (%)	under (+)/over (−) estimation of silica particles (%)
2	1.71×10^{16}	6.75×10^{16}	11.45	−14.54	−2473.67
10	9.12×10^{16}	4.40×10^{15}	10.18	−1.77	−67.66
14	$\mathbf{9.63 \times 10^{16}}$	$\mathbf{2.61 \times 10^{15}}$	**9.99**	**0.10**	**0.68**
20	1.04×10^{17}	1.36×10^{15}	9.88	1.21	47.11
50	1.25×10^{17}	1.96×10^{14}	10.16	−1.61	92.73

[a] In the model, the radius of the free micelles (=radius of adsorbed micelles) is taken as 19.1 Å (radii follow a log-normal distribution with $\sigma = 0.28$). The error in surfactant concentration and number density of particles for the fit parameters relative to the experimental values are also indicated.

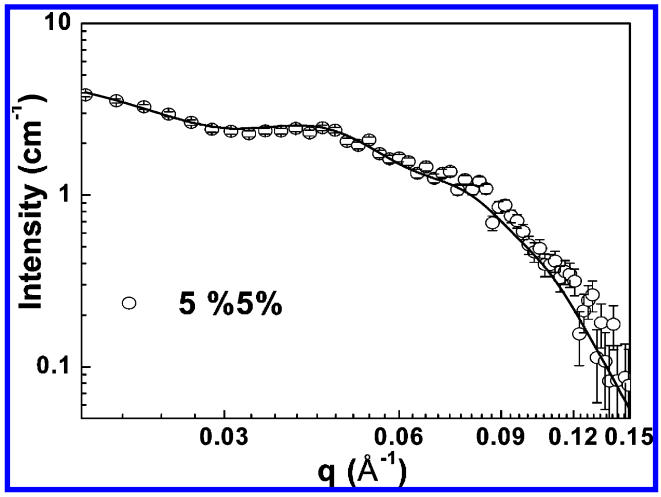

Figure 7. SANS for 5%5% sample (room temperature), showing the fit (solid line) to the adsorbed micelle model for $n_a = 14$.

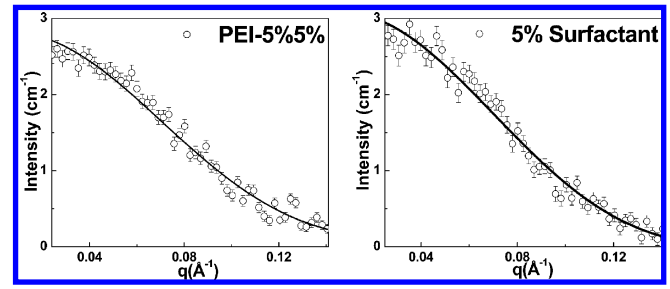

Figure 8. SANS (at room temperature) for (a) PEI-5%5% and (b) 5% surfactant samples in 40:60 H_2O:D_2O matrix, contrast matched to the scattering length density of silica.

4). In addition, the surfactant surface coverage estimated from this model is 1.5 mg·m^{-2}, in reasonable agreement with the value expected from adsorption isotherm data (see the Supporting Information). Thus, we believe that the structure of the surfactant/silica nanoparticle dispersion is most accurately described by an adsorbed micelle model, with an average of 14 surfactant micelles adsorbed on the surface of each nanoparticle. Within the accuracy of our scattering data, we believe that the adsorbed micelles are similar to those in solution.

We now examine the 5%5% sample and fit the adsorbed micelle model, represented by eq 6 to the scattering data. When we assume $\hat{S}_{pp}(q) = 1$, we are unable to fit the data for any value of n_a. As the nanoparticles with micelles adsorbed on them are large ($=2R_o + 2R_m$) and at a relatively high concentration (5% by weight of the nanoparticles in the dispersion), it is reasonable that we have to account for the interference between the scattering from these structures. We assume the simplest model to account for the interaction between the micelle covered nanoparticles, viz., a hard sphere potential, and calculate $\hat{S}_{pp}(q)$ accordingly. Again, for $n_a = 14$, the scattering data fits well (Figure 7), the surfactant concentration calculated from the fit matches closely with the experimental value, and the number density of silica nanoparticles closely matches that expected for a 5% dispersion of particles (Table 5, and see the Supporting Information for detailed calculations). The fit to $\hat{S}_{pp}(q)$ yields reasonable values (Table 5) for the hard sphere radius of the surfactant micelle adsorbed silica particles (119.6 Å $\approx R_o + 2R_m$) and for the volume fraction [$0.27 \approx \phi(R_o + 2\acute{R}_m)^3/R_o^3$, where $\phi = 0.023$ is the volume fraction of the silica nanoparticles, and $\acute{R}_m$ is the radius of the adsorbed surfactant micelle (estimated as ≈47 Å); $\acute{R}_m$ includes the hydrophobic core (R_m) and, the solvated ethylene oxide segments].

In the final part of this work, we examine the structure of polyethyleneimine (PEI) coated silica particles in surfactant solutions. We have previously shown that PEI with a molecular weight of 2000 g·mol^{-1} adsorbs on the surface of S15 and that zeta potential measurements indicate a reversal in the mean zeta potential from −33.5 mV for the S15 to +8 mV for the PEI−S15. From SAXS of 1% (by weight) PEI−S15, we obtained a particle radius/standard deviation of 81 Å/0.15 (marginally higher than for the S15, 74.5 Å/0.14, Figure S4 in the Supporting Information). Taken together, our data indicates that the PEI coats the S15, forming a monolayer on the surface of the silica nanoparticle. SANS from 5% (by weight) PEI−S15 in 5% (by weight) $C_{12}E_9$ (that we call the PEI-5%5% sample) in a water/D_2O 40/60 mixture that contrast matches the silica is presented in Figure 8a. A comparison between scattering profiles from 5%5% (Figure 7) and PEI-5%5% (Figure 8a) and from a 5% surfactant solution (Figure 8b) clearly indicates that the scattering profiles look similar for the 5% surfactant solution

TABLE 5: Fit Parameters for the Adsorbed Micelle Model (Figure 6) for $n_a = 14$[a]

n_a (5%5% sample)	$R_m = R_a$ (Å)/σ	ν_m (cm^{-3})	ν_p (cm^{-3})	R_{HS} (Å)	ϕ	calculated surfactant concentration (mg/mL)	under (+)/over (−) estimation of surfactant concentration (%)	under (+)/over (−) estimation of silica particles (%)
14	19.1/0.28	4.65×10^{17}	1.33×10^{16}	119.6	0.27	49.05	+1.91	−1.73

[a] The error in surfactant concentration and number density of particles for the fit parameters relative to the experimental values are also indicated.

TABLE 6: Parameters from Fitting SANS Data from PEI-5%5% (Figure 8a) and 5% Surfactant (Figure 8b)

sample	R_m (Å)	σ	ν_m (cm^{-3})
PEI-5%5%	20.3	0.3	8.7×10^{17}
5% $C_{12}E_9$	19.1	0.24	9.8×10^{17}

and PEI-5%5%, and that there is a qualitative difference in the shape of the scattering profile for the 5%5% sample. Specifically, the dip in the scattered intensity near $q = 0.04$ $Å^{-1}$ observed for the 5%5% sample is absent for PEI-5%5%. This suggests that adsorption of the PEI on S15 prevents adsorption of the surfactant micelles. We model the scattered data from the PEI-5%5% solution using the form factor for dilute polydisperse spheres and obtain a mean radius of 20.3 Å, and a standard deviation of 0.3 (Figure 8a, Table 6). This compares well with the values from fitting the scattering from 5% surfactant solution (mean radius = 19.1 Å, standard deviation = 0.24; Figure 8b, Table 6). Thus, scattering from PEI-5%5% in solvent contrast matched to silica is dominated by the scattering from surfactant micelles and the PEI−S15 particles do not appear to contribute much to the scattering. We have previously shown that nanoparticulate networks, formed by PEI−S15 particles that phase separate from $C_{12}E_9$ solutions, can be cross-linked using agents that create bonds that link PEI molecules and that these cross-linked PEI−S15 scaffolds are self-standing, even after removal of the surfactant. In contrast, particulate networks of the S15 are thermoreversible, and redisperse on surfactant removal, or on heating the surfactant into the isotropic micellar phase. Our SANS data provide us with an understanding of the mechanism for this behavior. $C_{12}E_9$ micelles adsorb on the surface of S15 particles and stabilize the particles against aggregation. The micelle adsorbed particle structures interact with each other through a hard sphere potential. In contrast, PEI coating the S15 particles prevents micellar adsorption, and provides a cross-linkable polymer coat to the S15 particles, thus allowing the formation of cross-linked and self-standing PEI−S15 nanoparticulate scaffolds.

Summary

Charge stabilized silica particles disperse readily in a 1:1 $C_{12}E_9$:water solution when mixed at high temperature (50 °C), in the isotropic micellar phase. An aqueous dispersion of the silica particles aggregates irreversibly when it is destabilized, for example, by increasing the ionic strength. However, interestingly, a dispersion of the same particles in 1:1 $C_{12}E_9$:water is stable even in brine, and over a range of pH values. SANS on particle dispersions in 1:1 $C_{12}E_9$:water, where the surfactant is contrast matched, reveals that the interparticle interaction can be modeled by a hard sphere interaction. Thus, the mean potential of interparticle interaction changes from a screened Coulombic potential in water to a hard sphere potential in 1:1 $C_{12}E_9$:water. SANS on dilute particle/surfactant solution reveals that the structure can be modeled as surfactant micelles adsorbed on the particle surface, with 14 micelles adsorbed on each particle, on average. We believe that these adsorbed micelles provide a steric repulsion between the particles that stabilizes them against irreversible aggregation, and gives rise to the hard sphere interparticle potential. The adsorbed micelles appear to be strongly associated with the silica particles. In particle dispersions in concentrated (viz., 1:1) $C_{12}E_9$:water solutions, cooling from 50 °C to room temperature results in the formation of a hexagonal (H_1) gel phase. H_1 domains exclude the silica particles, and these nanoparticles phase separate to form scaffolds. This particle aggregation to form scaffolds is thermoreversible, and the particles redisperse on heating into the micellar phase. This suggests that, even when the particles phase aggregate at the H_1 domain boundaries, surfactant micelles remain associated with the particles, rendering the aggregation thermoreversible. Coating the silica particles by adsorbing an oppositely charged polyelectrolyte, PEI, prevents surfactant adsorption on the particle surface.

Acknowledgment. K.P.S gratefully acknowledges a research fellowship from CSIR India and the SANS facility at the Bhabha Atomic Research Center at Mumbai.

Supporting Information Available: Figures showing SAXS and SANS spectra and $\hat{S}_{aa}(q)$ data, tables showing fitting parameters, and calculations from both of the models used in this investigation. This material is available free of charge via the Internet at http://pubs.acs.org.

References and Notes

(1) Sharma, K. P.; Kumaraswamy, G.; Ly, I.; Mondain-Monval, O. *J. Phys. Chem. B* **2009**, *113* (11), 3423–3430.

(2) (a) Fabre, P.; Cassagrande, C.; Veyssie, M.; Cabuil, V.; Massart, R. *Phys. Rev. Lett.* **1990**, *64*, 539. (b) Quilliet, C.; Ponsinet, V.; Cabuil, V. *J. Phys. Chem.* **1994**, *98*, 3566–3569. (c) Eiser, E.; Bouchama, F.; Thathagar, M. B.; Rothenberg, G. *ChemPhysChem* **2003**, *4*, 526. (d) Bouchama, F.; Thathagar, M. B.; Rothenberg, G.; Turkenburg, D. H.; Eiser, E. *Langmuir* **2004**, *20*, 477–483. (e) Wadekar, M. N.; Pasricha, R.; Gaikwad, A. B.; Kumaraswamy, G. *Chem. Mater.* **2005**, *17*, 2460.

(3) Holmberg, K., Shah, D. O., Schwuger, M. J., Eds. *Handbook of Applied Surface and Colloid Chemistry*; John Wiley: New York, 2002.

(4) McDermott, D. C.; Lu, J. R.; Lee, E. M.; Thomas, R. K.; Rennie, A. R. *Langmuir* **1992**, *8* (4), 1204–1210.

(5) Bohmer, M. R.; Koopal, L. K.; Janssen, R.; Lee, E. M.; Thomas, R. K.; Rennie, A. R. *Langmuir* **1992**, *8* (9), 2228–2239.

(6) Tiberg, F.; Jonsson, B.; Tang, J.; Lindmann, B. *Langmuir* **1994**, *10* (7), 2294–2300.

(7) Howse, J. R.; Steitz, R.; Pannek, M.; Simon, P.; Schubert, D. W.; Findenegg, G. H. *Phys. Chem. Chem. Phys.* **2001**, *3*, 4044–4051.

(8) Matsson, M. K.; Kronberg, B.; Claesson, P. M. *Langmuir* **2004**, *20* (10), 4051–4058.

(9) (a) Levitz, P.; Damme, H. V.; Keravis, D. *J. Phys. Chem.* **1984**, *88* (11), 2228–2235. (b) Levitz, P.; Damme, H. V. *J. Phys. Chem.* **1986**, *90* (7), 1302–1310. (c) Levitz, P.; Damme, H. V. *J. Phys. Chem.* **1986**, *90* (7), 1302–1310.

(10) Qiao, Y.; Schönhoff, M.; Findenegg, G. H. *Langmuir* **2003**, *19* (15), 6160–6167.

(11) Findenegg, G. H.; Eltekov, A. Y. *J. Chromatogr., A* **2007**, *1150*, 236–240.

(12) Dietsch, O.; Eltekov, A. Y.; Bock, H.; Gubbins, K. E.; Findenegg, G. H. *J. Phys. Chem. C* **2007**, *111* (43), 16045–16054.

(13) (a) Cummins, P. G.; Staples, E.; Penfold, J. *J. Phys. Chem.* **1990**, *94* (9), 3740–3745. (b) Cummins, P. G.; Penfold, J.; Staples, E. *Langmuir* **1992**, *8* (1), 31–35. (c) Penfold, J. *J. Phys. Chem.* **1996**, *100* (46), 18133–18137.

(14) Giordano-Palmino, F.; Denoyel, R.; Rouquerol, J. *J. Colloid Interface Sci.* **1994**, *165*, 82–90.

(15) Despert, G.; Oberdisse, J. *Langmuir* **2003**, *19* (18), 7604–7610.

(16) Levitz, P.; Miri, A. E.; Keravis, D.; Damme, H. V. *J. Colloid Interface Sci.* **1984**, *99* (2), 484–492.

(17) Dong, J.; Mao, G. *Langmuir* **2000**, *16* (16), 6641–6647.

(18) Patrick, H. N.; Warr, G. G.; Manne, S.; Aksay, I. A. *Langmuir* **1997**, *13* (16), 4349–4356.

(19) Grant, L. M.; Tiberg, F.; Ducker, W. A. *J. Phys. Chem. B* **1998**, *102* (22), 4288–4294.

(20) (a) Tiberg, F.; Brinck, J.; Grant, L. *Curr. Opin. Colloid Interface Sci.* **1999**, *4*, 411–419. (b) Warr, G. G. *Curr. Opin. Colloid Interface Sci.* **2000**, *5*, 88–94.

(21) Duits, M. H. G.; May, R. P.; Vrij, A.; de Kruif, C. G. *J. Chem. Phys.* **1991**, *94* (6), 4521–4531.

(22) Lee, E. M.; Thomas, R. K.; Cummins, P. G.; Staples, E.; Penfold, J.; Rennie, A. R. *Chem. Phys. Lett.* **1989**, *162* (3), 196–202.

(23) Oberdisse, J. *Phys. Chem. Chem. Phys.* **2004**, *6*, 1557–1561.

(24) Lugo, D.; Oberdisse, J.; Karg, M.; Schweins, R.; Findenegg, H. *Soft Matter* **2009**, *5*, 2928–2936.

(25) Alexeev, V. L.; Ilekti, P.; Persello, J.; Lambard, J.; Gulik, T.; Cabane, B. *Langmuir* **1996**, *12*, 2392–2401.

(26) Wadekar, M. N.; Pasricha, R.; Gaikwad, A. B.; Kumaraswamy, G. *Chem. Mater.* **2005**, *17*, 2460.

(27) Bringley, J. F.; Wunder, A.; Howe, A. M.; Wesley, R. D.; Qiao, T. A.; Liebert, N. B.; Kelley, B.; Minter, J.; Antalek, B.; Hewitt, J. M. *Langmuir* **2006**, *22*, 4198–4207.

(28) Aswal, V. K.; Goyal, P. S. *Curr. Sci.* **2000**, *79* (7), 947–953.

(29) SASfit vers. 0.90.1 software by Joachim Kohlbrecher, Laboratory for Neutron Scattering, PSI, Switzerland.http://kur.web.psi.ch/sans1/SANSSoft/sasfit.html.

(30) Kaler, E. W. Small-Angle Scattering from Complex Fluids. *Modern Aspects of Small-Angle Scattering*; Brumberger, H., Ed.; Kluwer Academic Publishers: Dordrecht, The Netherlands, 1993; pp 329−353.

(31) Kline, S. R.; Kaler, E. W. *J. Chem. Phys.* **1996**, *105* (9), 3813–3822.

(32) (a) Qiu, D.; Cosgrove, T.; Howe, A. M.; Dreiss, C. A. *Langmuir* **2006**, *22*, 546–552. (b) Ramsay, J. D. F.; Avery, R. G.; Benest, L. *Faraday Discuss. Chem. Soc.* **1983**, *76*, 53–63.

(33) Israelachvili, J. N. *Intermolecular and Surface Forces*, 2nd ed.; Academic Press Limited: London, 1992.

(34) Hayter, J. B.; Penfold, J. *Mol. Phys.* **1981**, *42*, 109.

(35) Penfold, J.; Ramsay, J. D. F. *J. Chem. Soc., Faraday Trans. 1* **1985**, *81*, 117–125.

(36) Jijo, V. J.; Sharma, K. P.; Kamble, S.; Rajamohanan, P. R.; Ajithkumar, T. G.; Badiger, M. V.; Kumaraswamy, G. *Macromolecules* **2010**, *43*, 4782–4790.

(37) (a) Mitchell, D. J.; Tiddy, G. J. T.; Waring, L.; Bostock, T.; McDonald, M. P. *J. Chem. Soc., Faraday Trans. 1* **1983**, *79*, 975–1000. (b) Kunieda, H.; Ozawa, K.; Huang, K.-L. *J. Phys. Chem. B* **1998**, *102*, 831.

(38) Vrij, A. *Pure Appl. Chem.* **1976**, *48*, 471.

(39) Levitz, P. *Langmuir* **1991**, *7*, 1595–1608.

JP1033799